J Appl Electrochem (2012) 42:209–215
DOI 10.1007/s10800-012-0390-8

ORIGINAL PAPER

Synthesis of LSM–YSZ–GDC dual composite SOFC cathodes for high-performance power-generation systems

Hyun Jun Ko · Jae-ha Myung · Sang-Hoon Hyun · Jong Shik Chung

Received: 5 December 2011 / Accepted: 6 February 2012 / Published online: 2 March 2012

Abstract This article investigates a method in further improvement of a $(La_{0.8},Sr_{0.2})MnO_3$ (LSM)-Yttria-stabilized zirconia (YSZ) dual composite cathode by adding material with high ionic conductivity such as gadolinia-doped ceria (GDC). A nano-porous composite cathode containing LSM, YSZ, and GDC was prepared by a two-step polymerizable complex (PC) method which minimizes the formation of YSZ–GDC solid solution. The structure of the resulting LSM/GDC–YSZ dual composite cathode was such that the LSM and GDC phases were present on the YSZ core particles without formation of the $La_2Zr_2O_7$, $SrZrO_3$, and GDC–YSZ solid solution. At 800 °C, the electrode polarization resistance of the LSM/GDC–YSZ dual composite cathode decreased to 0.266 Ω cm^2, compared with 0.385 Ω cm^2 for the LSM/YSZ–YSZ dual composite cathode. In addition, the Ni–YSZ anode-supported single cell using a LSM/GDC–YSZ dual composite cathode with H_2 as the fuel achieved a maximum power density of 0.65 W cm^{-2} at 800 °C.

Keywords Solid oxide fuel cell · Composite cathode · PC method · LSM · GDC · YSZ

H. J. Ko · J. Myung · S.-H. Hyun (✉)
School of Advanced Materials Science and Engineering, Yonsei University, Seoul 120-749, Korea
e-mail: prohsh@yonsei.ac.kr

J. S. Chung
Department of Chemical Engineering, Pohang University of Science and Technology, San 31, Hyoja-dong, Nam-ku, Pohang 790-784, Korea

1 Introduction

Solid oxide fuel cells (SOFCs) have attracted attention as a next generation power-generation system because of their high efficiency and reduced emissions. For the practical use of SOFCs, it is essential to achieve a high-power density and long-term stability for over 10,000 h at intermediate temperatures (650–800 °C). However, existing SOFCs are associated with problems such as interfacial diffusion, thermal mismatch, and large electrode (anode, cathode) overpotential [1–5, 17]. A possible solution involves lowering cathodic overpotential, which consumes a large portion of the total polarization, through the synthesis of nano-sized cathode materials that extend the triple-phase boundary (TPB). To this end, nano-porous $La_{0.8}Sr_{0.2}MnO_3$ (LSM) perovskite—$Y_{0.08}Zr_{0.92}O_{1.96}$ (YSZ) cathodes are promising cathode materials because of their strong electrochemical activity, good compatibility with YSZ electrolytes, and chemical stability in oxidizing atmospheres at high temperatures (>800 °C) [5–7]. However, it is difficult to achieve high performance with commercial LSM–YSZ composite cathodes because of their small effective surface area for electrocatalytic reactions. To improve the electrocatalytic activity, a LSM/YSZ–YSZ dual composite cathode has been previously studied and analyzed, in which both LSM and YSZ particles were conjugated on the YSZ-core particles [5–7]. The results confirmed that the cathodic performance and durability were progressed by the improved phase contiguity and interfacial coherence. One method for further improving the LSM/YSZ–YSZ composite cathode performance is to add ionic conducting materials such as GDC instead of YSZ to form a LSM/GDC–YSZ dual composite cathode [8].

There are many techniques for the synthesis of nano-composite materials, including impregnation [8], coprecipitation

[9], amorphous citrate [10], polymeric gel [11], and polymerizable complex (PC) methods [12]. In this study, LSM/GDC–YSZ dual composite materials were synthesized, with LSM and GDC phases deposited on the YSZ core particles, using the PC method based on polyesterification between citric acid (CA) and ethylene glycol (EG). Previous studies show that LSM/YSZ–YSZ dual composite cathode with a composition ratio of 50:10:40 wt% (47:11:42 vol%) have low polarization resistance and good stability [7]. Hence, according to the fact that YSZ and GDC share the same cubic phase structures, the 50:10:40 wt% composition ratio has been accordingly used of the LSM/GDC–YSZ dual composite particles in this study. The polarization resistance and the durability of the LSM/GDC–YSZ dual composite cathode were then investigated to verify the effects of adding GDC in place of YSZ. In addition, the fuel cell performance of Ni–YSZ anode-supported single cells with LSM/GDC–YSZ cathode was evaluated.

2 Experiment

2.1 Synthesis of LSM/GDC–YSZ dual composite powder

The LSM/GDC–YSZ dual composite powder was prepared by a two-step polymerizable complex method to minimize the formation of GDC–YSZ solid solution which decreases the ionic conductivity [32, 33]. The experimental procedure is described in detail in Fig. 1. In brief, stoichiometric amounts of the nitrate metal salts La, Sr, and Mn were dissolved with citric acid in de-ionized water at 70 °C for 1 h, after which ethylene glycol and YSZ ($\sim$0.3 μm, 6.2 $m^2\ g^{-1}$) core particles were added to the solution. The resulting mixture was then heated at 120 °C for 5 h to remove excess water and to achieve polyesterification between the metal ions (La, Sr, and Mn), the citric acid, and the ethylene glycol. LSM–YSZ single nano-composite powders were obtained after calcination at 800 °C. To obtain the LSM/GDC–YSZ dual composite powders, experiments using LSM–YSZ single composite powders as core particles were performed with nitrate salts of Gd and Ce. The powders were characterized to identify the crystalline phases without formation of the secondary phases such as $La_2Zr_2O_7$, $SrZrO_3$, and GDC–YSZ solid solution by X-ray diffraction (XRD, Ringaku). The surface area of LSM/GDC–YSZ powders was measured to identify the increase of reaction site by Brunauer–Emmer–Teller (BET, Micrometrics ASAP 2020) method. Then, the microstructure and composition distribution of LSM/GDC–YSZ composite powders were analyzed by a transmission electron microscope (TEM, JEOL), a scanning electron microscope (SEM, FEI), and energy dispersive spectroscopy (EDS, FEI). Moreover, an electrophoretic light scattering spectrophotometer (ELS, Otsuka electronics) was used for observing the surface charge of the powder to

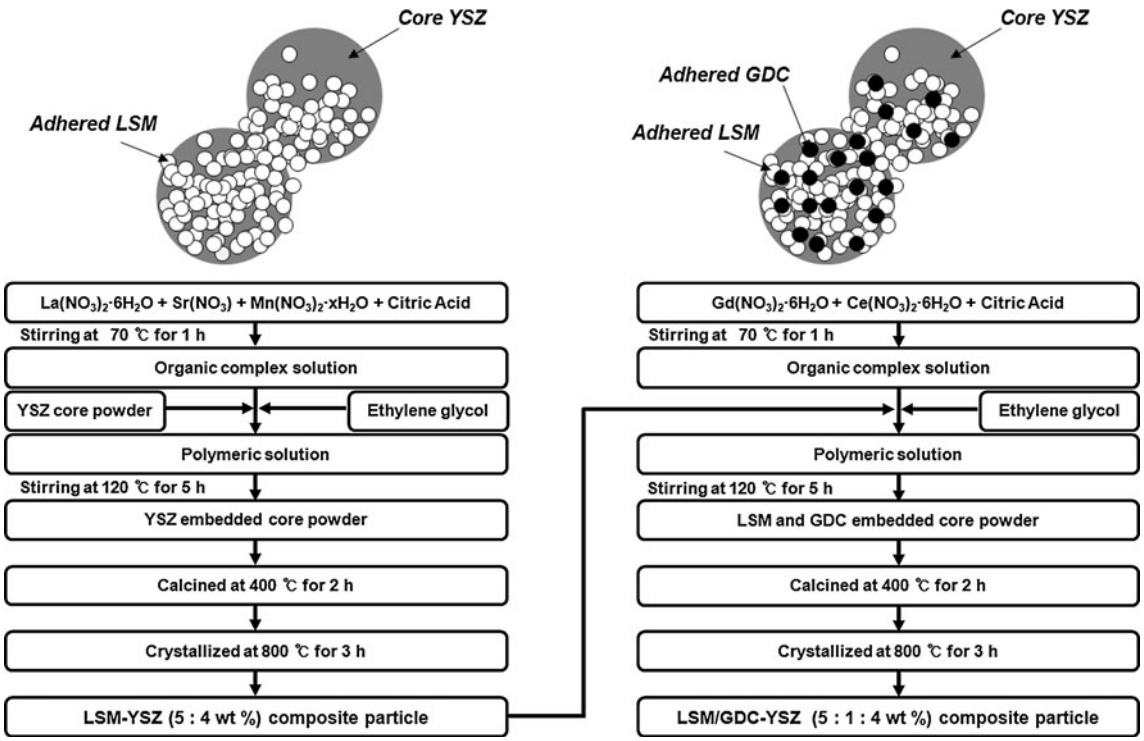

Fig. 1 Images of the ideal structure of nano-composite powders and flow charts for the synthesis of the LSM/GDC–YSZ dual composite powder

determine the existence of conjugated nano-sized particles on core particles [28].

2.2 Electrical analysis and performance evaluation of LSM/GDC–YSZ dual composite cathode

Symmetrical cells (LSM/GDC–YSZ//YSZ electrolyte// LSM/GDC–YSZ) were constructed to evaluate the performance of the LSM/GDC–YSZ dual composite cathode materials. Cathode layers were deposited on YSZ disks (sintered at 1400 °C for 3 h) by screen printing and were fired at 1100, 1150, 1200, and 1250 °C. Electrochemical impedance measurements were performed on the symmetrical cells under an air atmosphere by ac impedance spectroscopy (Solartron SI 1260/1287) and cathode durability tests were performed according to the schedule shown in Fig. 2 [18–23].

Ni–YSZ anode-supported cells with LSM/GDC–YSZ dual composite cathode were also fabricated. NiO–YSZ anode supports were prepared by pressing and were pre-sintered at 1200 °C. YSZ electrolytes with thickness of 6–7 μm were dip-coated onto the anode support. After sintering at 1350 °C for 3 h, one side of the support was polished to remove the YSZ electrolyte, after which the LSM/GDC–YSZ dual composite cathode materials were screen printed on the YSZ electrolyte and sintered at 1200 °C. The performance of the Ni–YSZ anode-supported unit cells was measured at 800 °C with H_2 as the fuel.

3 Results and discussion

3.1 Characteristics of LSM/GDC–YSZ dual composite powder

Figure 3 shows the XRD patterns of commercial YSZ, GDC, LSM, and the synthesized LSM/GDC–YSZ dual composite particles. The peaks of the LSM/GDC–YSZ

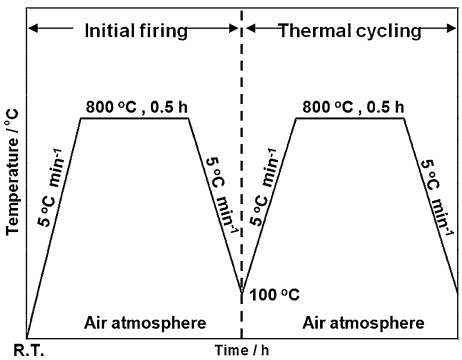

Fig. 2 Thermocycle test schedule

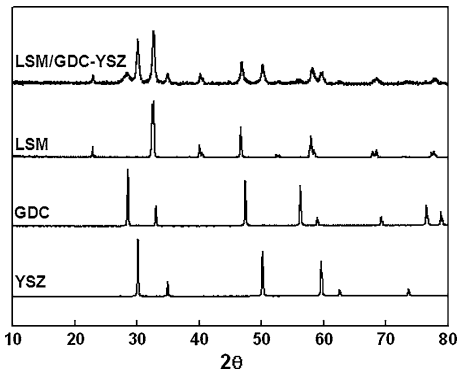

Fig. 3 XRD patterns for commercial YSZ, GDC, LSM, and the synthesized LSM/GDC–YSZ dual composite powder as calcined at 800 °C

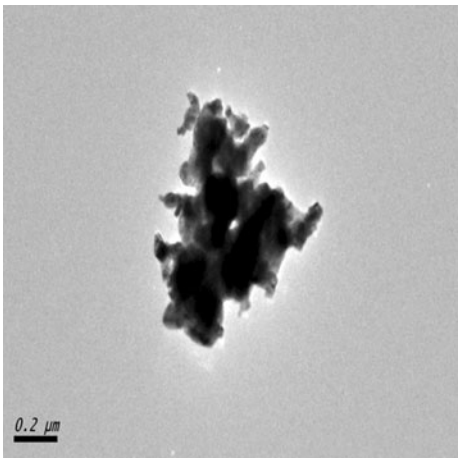

Fig. 4 TEM image of the LSM/GDC–YSZ dual composite powder

particles were compared with the commercial YSZ, GDC, and LSM peaks to detect the formation of secondary phases; only the primary phases, including the LSM perovskite, YSZ cubic, and GDC cubic phases, were observed. From the XRD results, formation of GDC–YSZ solid solution was successfully suppressed by the two-step pc method. As shown in Fig. 4, the LSM/GDC–YSZ dual composite particles were present as agglomerates of ~600 nm. Moreover, nano-sized particles (20–30 nm) were tightly linked with the YSZ core particles. To obtain detailed information about the existence of conjugated nano-particles, the surface charge of commercial YSZ core particles and synthesized LSM/GDC–YSZ composite particles were characterized by using ELS, which evaluate the zeta potential and profile of the electroosmotic stream plot (EOS plot). From Fig. 5, the surface charge was changed from 48.16 mV (YSZ) to −39.62 mV (LSM/GDC–YSZ) because the nano-sized particles are coated on the YSZ-core particle. Moreover, it was found that the conjugated

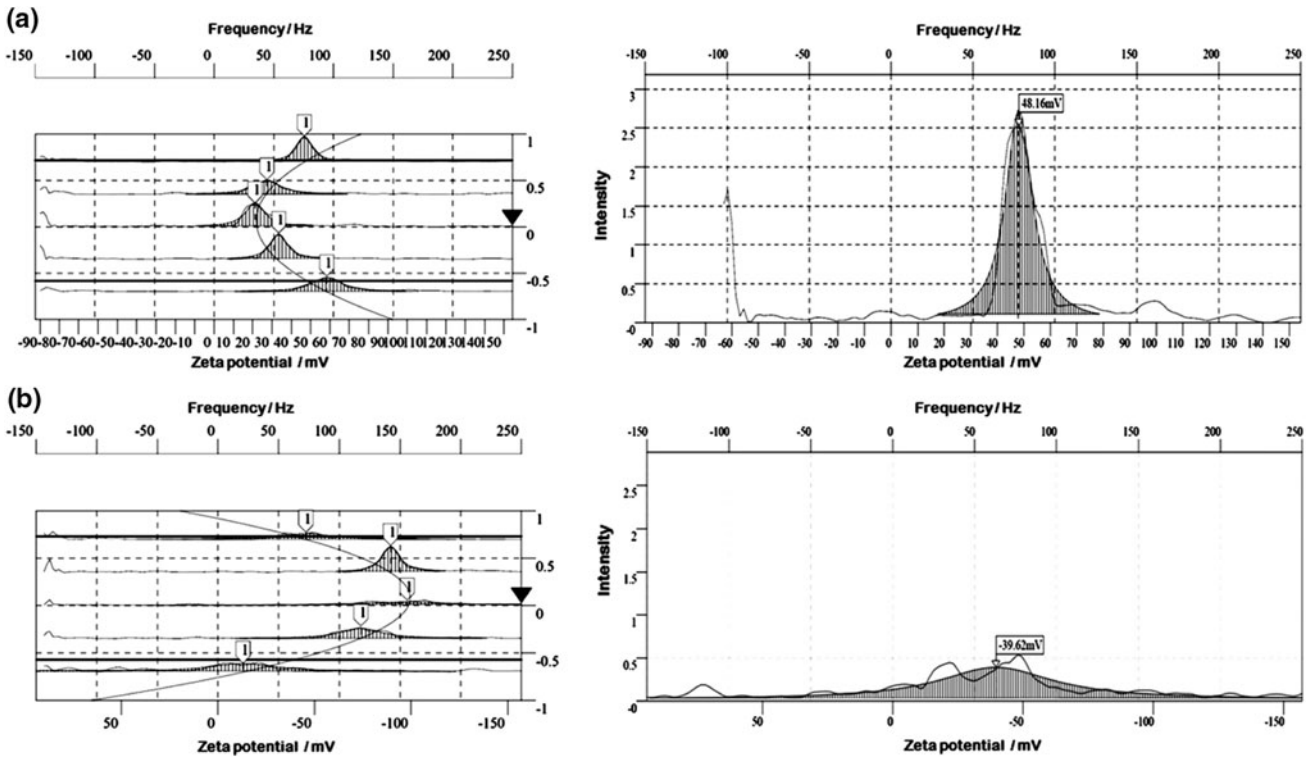

Fig. 5 EOS plots and the surface charges of (**a**) commercial YSZ, (**b**) synthesized LSM/GDC–YSZ dual composite powder

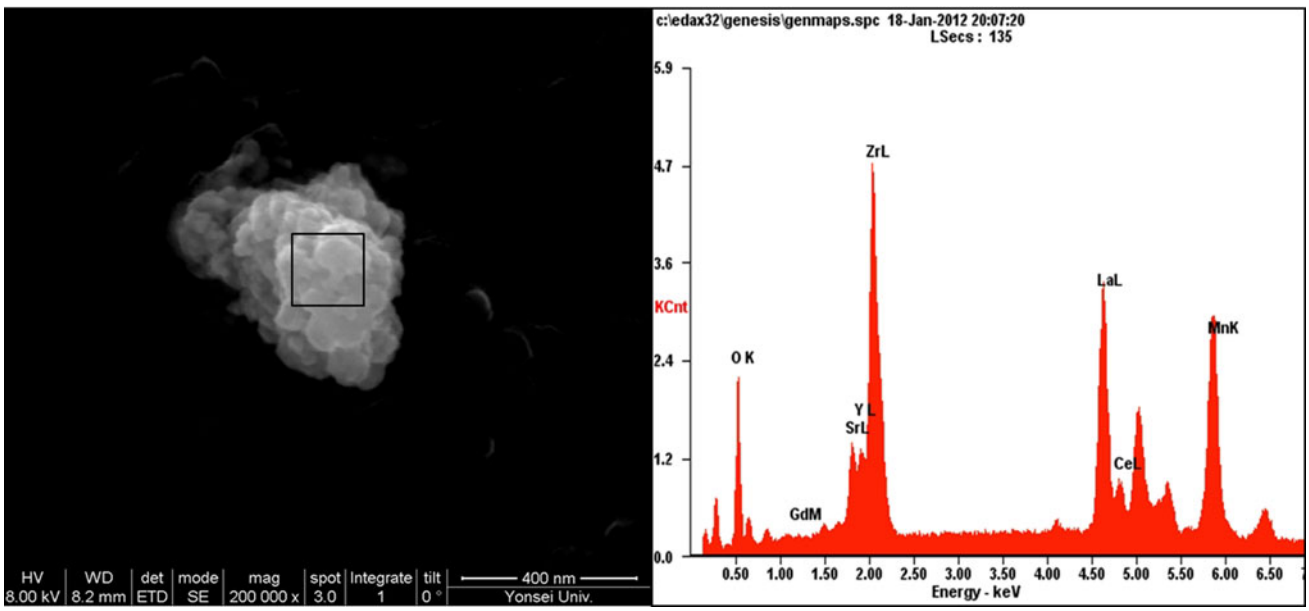

Fig. 6 SEM-EDS data for the LSM/GDC–YSZ dual composite powder

particles were well dispersed due to the parabolic shape of the LSM/GDC–YSZ particles as shown in the Fig. 5b [28]. Finally, it was verified that the conjugated nano-sized particles were LSM and GDC phases, by the SEM-EDX (Fig. 6).

3.2 Performance evaluation of the LSM/GDC–YSZ dual composite cathode

Figure 7a shows the total interfacial polarization resistances of symmetrical cells of the LSM/GDC–YSZ dual composite

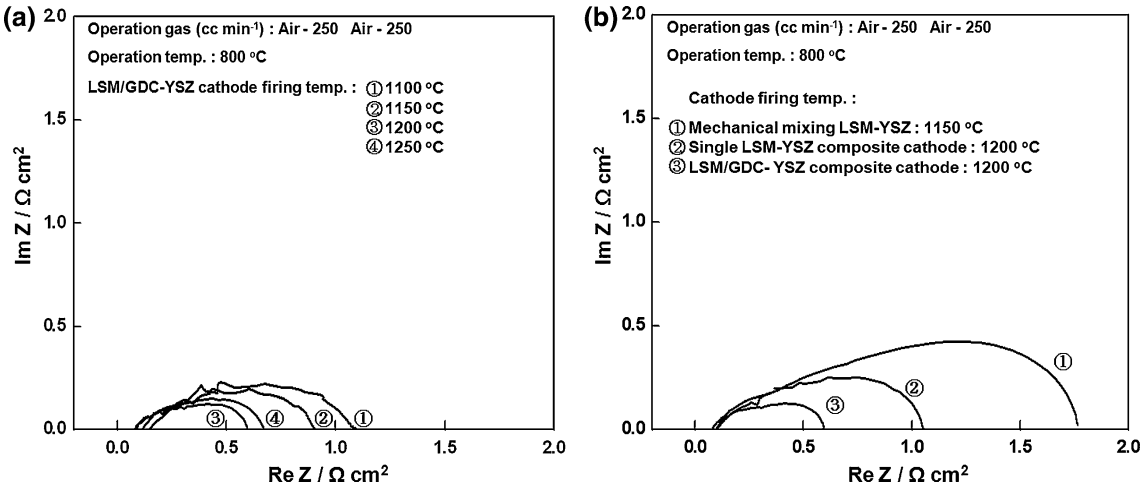

Fig. 7 Electrode polarization resistances of the LSM/GDC–YSZ dual composite cathode with respect to cathode firing temperature (**a**) and compared with commercial LSM–YSZ and LSM–YSZ single composite cathodes (**b**)

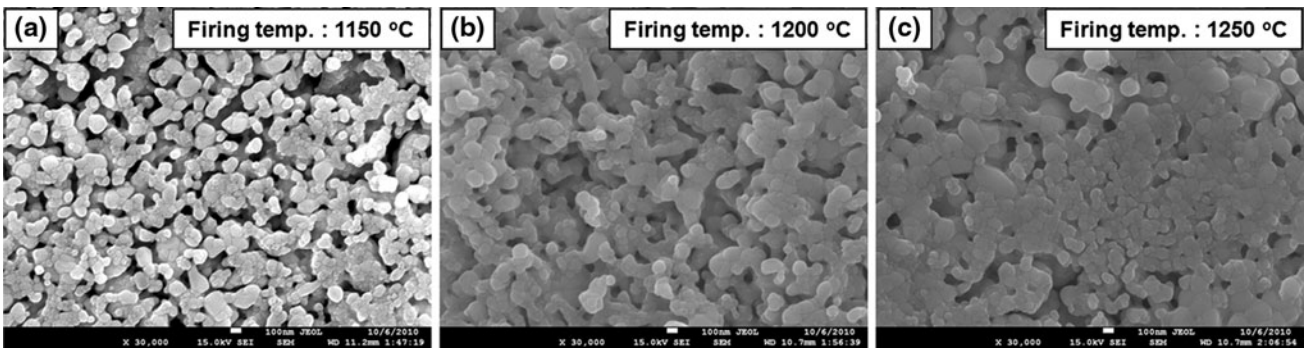

Fig. 8 SEM images of the LSM/GDC–YSZ dual composite cathode after firing at (**a**) 1150 °C, (**b**) 1200 °C, and (**c**) 1250 °C

cathode with respect to the cathode firing temperature. The polarization resistance of the cathode is signified as half of the total interfacial polarization resistance because the symmetrical cell is composed of two symmetrical electrodes [27]. Therefore, the polarization resistance of the LSM/GDC–YSZ dual composite cathodes fired at 1100, 1150, 1200, and 1250 °C were 0.480, 0.402, 0.266, and 0.299 Ω cm^2, respectively. From Fig. 8a, the low connectivity between cathode particles, which were fired under the 1200 °C, could explain the high-polarization resistance. However, there are two possible reasons which lead to increase of the polarization resistance of the cathode fired at 1250 °C. One is that over-sintered cathode particles deteriorate the cathode pore structure which is related to the mass transport overpotential as seen in Fig. 8c. The other possible reason is that the formation of the secondary phase reaction between LSM and YSZ mostly occurs at high temperature [13–16]. According to previous research findings the secondary phase of $La_2Zr_2O_7$ and $SrZrO_3$, which has a large negative effect on the cathodic performance, occurs at 1400 °C [29]. The structure change of LSM phases within the LSM/GDC–YSZ particles was analyzed by according to the cathode firing temperature because the temperature when the secondary phases are formed could be lowered due to the high activity of nano-sized particles. As shown in Fig. 9, there are not any peak differences compared to the calcined LSM phases, even though the sintering temperature of LSM/GDC–YSZ cathode is increased to 1300 °C. Also, the lattice parameters of the LSM phases in the LSM/GDC–YSZ particles are listed in Table 1. The LSM phases mostly maintained perovskite structures with monoclinic unit cells, with negligible distortion of the cubic perovskite structure [30, 31]. This can be explained by the fact that the rapid microstructure change brings the increase of polarization resistance of the cathode which was fired at 1250 °C not causing by the formation of secondary phases. Therefore, the lowest electrode polarization resistance value was 0.266 Ω cm^2 for the cathode that was fired at 1200 °C; this polarization resistance was lower than that of either the commercial LSM–YSZ cathode (0.895 Ω cm^2) or the LSM–YSZ single composite cathode (0.487 Ω cm^2), as shown in Fig. 7b. In particular, the

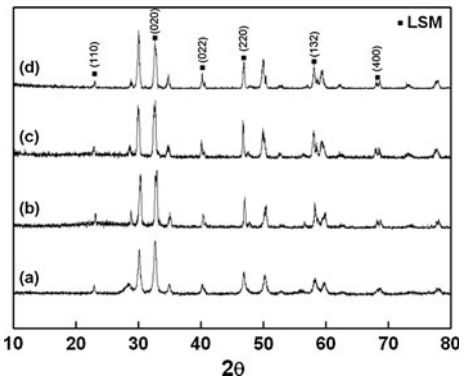

Fig. 9 XRD patterns for LSM/GDDC–YSZ dual composite cathode with respect to cathode firing temperature (**a**) as calcined at 800 °C (**b**) as fired at 1200 °C, (**c**) 1250 °C, and (**d**) 1300 °C

Table 1 The lattice parameters of LSM within the LSM/GDC–YSZ particles depending on cathode firing temperature (a) as calcined at 800 °C (b) as fired at 1200 °C, (c) 1250 °C, and (d) 1300 °C

	a/Å	b/Å	c/Å	ß/°
a	6.119	5.550	8.667	90.005
b	6.102	5.420	8.841	90.002
c	6.135	5.509	8.695	90.003
d	6.138	5.456	8.813	90.001

electrode polarization resistance of the LSM/GDC–YSZ dual composite cathode was reduced by over one-third in comparison with the commercial LSM–YSZ cathode, indicating that the synthesized cathode which has high-surface area (16.141 $m^2\ g^{-1}$) could extend the TPB reaction sites to improve the electrochemical performance [24]. Moreover, the electrode polarization resistance of the LSM/GDC–YSZ dual composite cathode was decreased by 30% in comparison with that of the LSM/YSZ–YSZ dual composite cathode (0.347 Ω cm^2) presumably because the GDC coating particles do not only have a higher ionic conductivity than YSZ, but also have a good catalysis to oxygen reduction at the process of cathode reaction [5–7]. Thermal cycle testing was performed to confirm the cathode stability. After completion of 30 thermal cycle tests, the electrode polarization resistance of the commercial LSM–YSZ cathode increased from 0.884 to 1.056 Ω cm^2 (19.8%). However, for the LSM/GDC–YSZ dual composite cathode, an increment from 0.226 to 0.292 Ω cm^2 (9.8%) occurred, as shown in Fig. 10. This result can be interpreted that the commercial LSM–YSZ composite cathode undergoes a considerable loss of YSZ phase interconnectivity between the electrode and the electrolyte or within the electrode during thermal cycle tests, bringing degeneration of the ionic conduction path. Moreover, reduction in TPB length could be caused by the coarsening of the LSM phase [6, 25, 26].

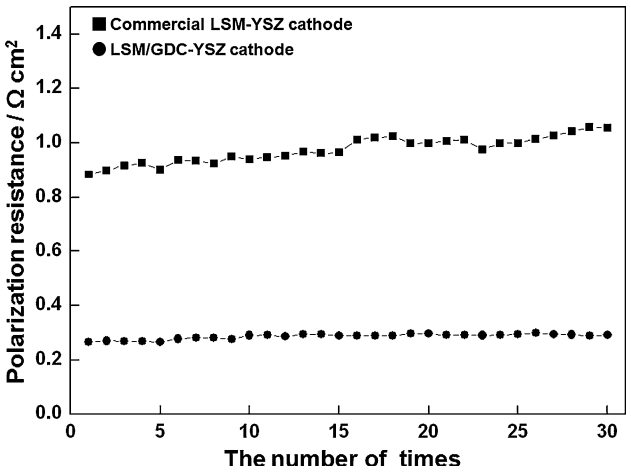

Fig. 10 Thermocycle test data for the commercial LSM–YSZ cathode and the LSM/GDC–YSZ dual composite cathode

The fuel cell performance of both the Ni–YSZ anode-supported single cells with the LSM/GDC–YSZ dual composite and the commercial LSM–YSZ cathode were evaluated at 800 °C with hydrogen as fuel. As shown in Fig. 11, a maximum power density of 0.37 W cm^{-2} was achieved for the commercial LSM–YSZ cathode, whereas the Ni–YSZ anode-supported single cell with a composite cathode exhibited a maximum power density of 0.65 W cm^{-2}.

4 Conclusion

To improve the electrochemical performance of the LSM/YSZ–YSZ dual composite cathode that has been previously developed, the effects of the coating material (GDC) on the LSM–YSZ composite cathodes were examined. The LSM/GDC–YSZ dual composite cathode materials have been successfully synthesized by using a two-step polymerizable complex method. The resulting materials have been shown to achieve high performance and durability in solid-oxide fuel cells. In symmetrical half cell tests at 800 °C, the electrode polarization resistance of the LSM/GDC–YSZ dual composite cathode showed to be 0.266 Ω cm^2, in comparison with that of 0.347 Ω cm^2 for the LSM/YSZ–YSZ dual composite cathode. Together these results indicate that the improvement of cathodic performance is caused by the addition of GDC nano-particles which have high ionic conductivity and good catalysis to oxygen reduction. After 30 thermal cycle tests, the electrode polarization resistance of the commercial LSM–YSZ cathode increased by 19.8%, but that of the LSM/GDC–YSZ dual composite cathode, only increased by 9.8%. In addition, a Ni–YSZ anode-supported single cell with the LSM/GDC–YSZ dual composite cathode was fabricated

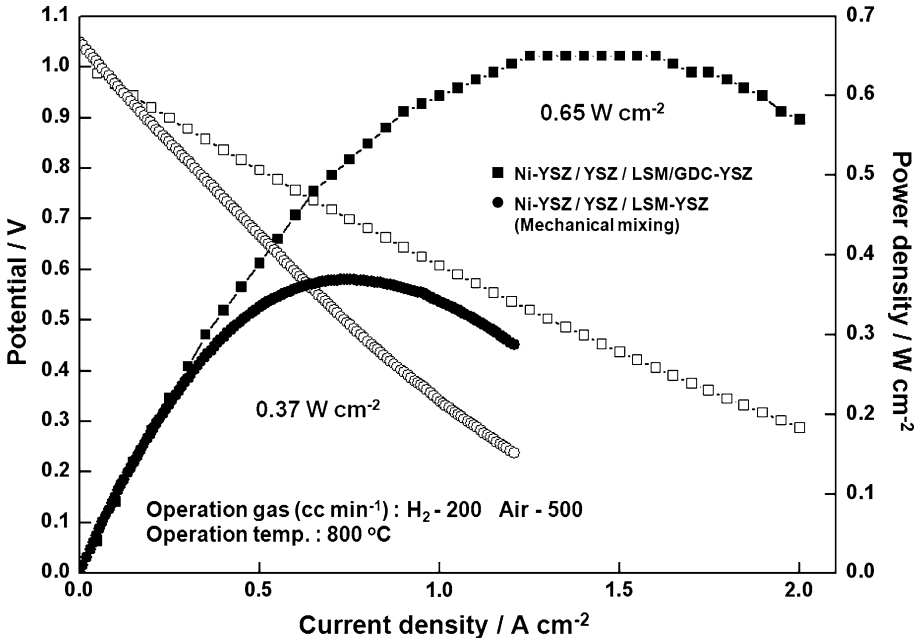

Fig. 11 Electrochemical performance of a Ni–YSZ anode-supported single cell with the LSM/GDC–YSZ dual composite cathode and the commercial LSM–YSZ cathode

and evaluated, achieving a maximum power density of 0.65 W cm^{-2} at 800 °C with H_2 as the fuel.

Acknowledgments This study was supported by a New & Renewable Energy grant of the Korea Institute of Energy Technology Evaluation and Planning (KETEP) funded by the Korean Ministry of Knowledge Economy (2009T100100344).

References

1. lvers-Tiffee E, Weber A, Herbstritt D (2001) Eur Ceram Soc 21:1805
2. Mogensen M, Skaarup S (1996) Solid State Ion 86/88:1151
3. lvers-Tiffee E, Weber A, Schmid K, Kerbs V (2004) Solid State Ion 174:223
4. Kuznecov M, Otschick P, Obenaus P, Eichler K, Schaffrath W (2003) Solid State Ion 157:371
5. Song HS, Lee S, Lee D, Kim H (2010) J Power Sources 195:2628
6. Song HS, Hyun SH, Kim J, Lee H-W, Moon J (2008) J Mater Chem 18:1087
7. Song HS, Lee S, Hyun SH, Kim J, Moon J (2009) J Power Sources 187:25–31
8. Jiang SP, Leng YJ, Chan SH, Khor KA (2003) Electrochem Solid-State Lett 6(4):A67
9. Nitadori T, lchiki T, Misono M (1988) Bull Chem Soc Jpn 61:621
10. Kremenic G, Nieto JML, Tascon JMD, Tejuca LG (1985) J Chem Soc Faraday Trans 81:939
11. Taguchi H, Matsuda D, Nagano M (1993) J Mater Sci Lett 12:891
12. Kakihana M, Arima M, Yoshimura M, Ikeda N, Sugitani Y (1999) J Alloy Compd 283:102
13. He H, Huang Y, Reagl J, Boaro M, Vohs JM, Gorte RJ (2003) J Am Ceram Soc 87(3):331
14. Takeda Y, Sakaki Y, Tu HY, Phillipps MB, Imanishi N, Yamamoto O (2000) Electrochemistry 68(10):764
15. Mitterdorfer A, Gauckler LJ (1998) Solid State Ion 111(3–4):185
16. Murata K, Shimotsu M (2002) J Ceram Soc Jpn 110(7):618
17. Cao H, Deng Z, Li X, Yang J, Qin Y (2010) Int J Hydrog Energy 35:1749
18. Kim YM, Kim-Lohsoontorn P, Baek SW, Bae J (2011) Int J Hydrog Energy 36:3138
19. Leng Y, Chan SH, Liu Q (2008) Int J Hydrog Energy 33:3808
20. Yang J, Muroyama H, Matsui T, Eguchi K (2010) Int J Hydrog Energy 35:10505
21. Yen-Pei F (2010) Int J Hydrog Energy 35:8663
22. Barbucci A, Paola Carpanese M, Viviani M, Vatistas N, Nicolella C (2009) J Appl Electrochem 39:513
23. Hjelm J, Sogaard M, Wandel M, Mogensen MB, Menon M, Hagen A (2007) ECS Trans 7(1):1261
24. Tanner CW, Fung K-Z, Virkar AV (1997) J Electrochem Soc 144(1):21
25. Adler SB, Lane JA, Steele BCH (1996) J Electrochem Soc 143(11):3554
26. Kim SD, Moon H, Hyun SH, Moon J, Kim J, Kim HW (2006) J Power Sources 163:392
27. Lee D, Jung I, Lee SO, Hyun SH, Jang JH, Moon J (2011) Int J Hydrog Energy 36:6875
28. Kim JA, Lee HJ, Kang H, Park TH (2009) Biomed Microdevices 11:287
29. Myung J, Ko HJ, Park H, Hyun MHSH (2012) Int J Hydrog Energy 36:498
30. Meng G, Song H, Xia C, Liu X, Peng D (2004) Fuel Cells 1–2:48
31. Ngyuen Q, Minh (1993) J Am Ceram Soc 76(3):563
32. Tsoga A, Gupta A, Naoumidis A, Nikolopoulos P (2008) Acta Mater 48:4709
33. Tsoga A, Naoumidis A, Stover D (2000) Solid State Ion 135:403